

1 **High efficiency** mid-infrared interband cascade LEDs grown on low
2 **absorbing substrates emitting > 5 mW of output power**

3
4 Nicolas Schäfer ^{a,*}, Julian Scheuermann ^a, Robert Weih ^a, Johannes Koeth ^a, Sven Höfling ^{b,c}
5

6 ^a nanoplus Nanosystems and Technologies GmbH, Gerbrunn, Germany

7 ^b Universität Würzburg, Technische Physik and Wilhelm Conrad Röntgen Research Center for Complex Material
8 Systems, Würzburg, Germany

9 ^c University of St. Andrews, Scottish Universities Physics Alliance, School of Physics and Astronomy, St. Andrews,
10 United Kingdom

11
12 * phone: +49-931-90827-21; email: nicolas.schaefer@nanoplus.com
13
14
15
16
17
18
19
20
21
22
23
24
25
26
27
28
29
30
31
32
33
34
35
36
37
38
39
40
41
42
43
44
45
46
47
48
49
50
51
52
53
54
55
56

57 Abstract

58
59 We present interband cascade light-emitting devices with incoherent and broadband light emission peaked at a
60 wavelength of around 3.7 μm . The substrate-side-emitting devices display higher wall plug efficiencies and
61 maximum output powers than any earlier mid-infrared LEDs operating in continuous wave at room temperature. To
62 reduce absorption losses, the epitaxial structures were grown on low doped (low absorbing) GaSb substrates. The
63 nine active stages were positioned in different configurations to investigate the impact of constructive or destructive
64 interference when reflected from the epitaxial-side metallization of the flip-chip mounted devices. A comparison
65 shows improved electrical properties and out-coupling efficiencies when all active stages are centered within a single
66 antinode of the optical field. The optimized voltage efficiency combined with low optical losses lead to a maximum
67 wall plug efficiency of 0.7 %. Flip-chip mounted devices with a 640 μm squared mesa reached output powers of up
68 to 5.1 mW at ambient temperatures with driving current (voltage) of 0.6 A (5.1 V).
69

70
71
72 Keywords

73
74 Interband cascade lasers, mid infrared lasers, light emitting devices, absorption spectroscopy, quantum cascade lasers
75
76
77

78 The growing demand for permanent monitoring of specific molecules in environmental, health and security
79 applications has created a need for inexpensive and power efficient light sources. Especially the mid-infrared (MIR)
80 wavelength range from 3 to 6 μm is of high interest for gas sensing applications. Compared to the near-infrared
81 spectral region many technologically and industrially relevant gas species have absorption features with orders of
82 magnitude higher absorbance in this wavelength region [1]. Interband cascade lasers (ICLs) have demonstrated
83 continuous-wave operation at temperatures well above ambient whilst still keeping low power consumption and are
84 thus well established light sources in the MIR spectral range [2].

85 However, for several applications and spectroscopic techniques, such as methane emission monitoring in agriculture
86 and dairy farming LEDs represent a broadband, incoherent but cost effective alternative to lasers.

87 Without the feedback from an optical cavity, the light emission of the presented interband cascade light-emitting
88 devices (ICLEDs) is not bound to a coherence or gain threshold. Similar to ICLs, the slope efficiency of these
89 devices can be increased by cascading multiple active stages in series, employing the GaSb/InAs broken gap
90 alignment and injector regions to transfer electrons from one emitting stage to the next.

91 Recent developments show that the efficiency can be further improved by centering the stages of substrate emitting
92 ICLEDs at the antinodes of the near-normal incidence optical field in the vicinity of a metal mirror [3].

93 However, due to low out-coupling efficiencies caused by total internal reflection at the high-index substrate to air
94 interface and absorption losses inside the n-doped GaSb substrate, the ICLEDs never exceeded wall plug efficiency
95 (WPE) of 0.4 % [3]. The two dominant sub-bandgap absorption mechanisms are free-carrier absorption by free
96 electrons and intervalley conduction-band absorption.

97 In this work, we present one effective approach to suppress free electron absorption losses by using low absorbing
98 substrates for substrate emitting ICLEDs.
99

100
101 The 9 stage ICLED structure was grown by molecular beam epitaxy (MBE) on low doped GaSb substrates. The
102 MBE system was equipped with valved cracker cells for the group V elements and conventional effusion cells for
103 group III elements and dopants. First of all a 500 nm thick GaSb:Te ($1 \cdot 10^{18} \text{ cm}^{-3}$) layer was grown to serve as
104 contact layer. As shown in figure 1, three different configurations were grown, which differ in the arrangement and
105 position of the active stages. While for the first structure all 9 active stages are centered on an antinode of the optical
106 field at normal incidence, the active cores of the second and third structure are partitioned in 3 groups each made of 3
107 active stages. The groups were separated and aligned by GaSb layers, so that each group is centered on antinode
108 (node) to meet the condition for constructive (destructive) interference, as shown in figure 1 and described in [3].
109

110 Square shaped ICLED mesa structures with edge lengths of $d = 640 \mu\text{m}$ were wet-etched using a
111 $\text{C}_6\text{H}_8\text{O}_7/\text{H}_3\text{PO}_4/\text{H}_2\text{O}_2/\text{H}_2\text{O}$ solution. To reduce the characteristic current spreading in superlattice like structures and
112 to improve the performance, the etch was proceeded throughout the active region. The etch depth had to be
113 controlled very precisely to hit the position of the 500 nm contact layer which is located directly underneath the

114 active core. It is crucial to reach an appropriate depth in order to ensure ohmic contacts with low contact resistance.
115 A Ti/Ag/Pt contact metallization was sputtered onto the topside of the mesa, additionally serving as a mirror with a
116 reflectivity of $\sim 94\%$ in the relevant wavelength range. The substrate-side AuGe/Ni/Au contact metallization was
117 sputtered ring-shaped around the mesa and onto a smaller second mesa to level both contacts for flip-chip mounting.
118 Subsequently, 50 nm of Si_3N_4 passivation layer were sputtered by plasma enhanced physical vapor deposition to
119 prevent short-circuiting the device during the flip-chip mounting, followed by an etch-back using a CHF₃-based
120 reactive ion etch process to open contact windows for both substrate and mesa contact. On top of the designated
121 contact areas 3-4 μm thick Au layers were electroplated to ensure sufficient heat removal and to serve as mounting
122 bumps.

123
124 Due to the absence of a waveguide, the spontaneously emitted light from an LED's active region can be considered
125 internally isotropic. However, only photons propagating within the critical angle for total-internal-reflection θ_c can
126 out-couple to the outer medium. For commercial LEDs emitting in the visible spectrum, θ_c is usually defined by the
127 planar interface between the semiconductor and a lens-shaped droplet of epoxy. However, epoxy is not transparent in
128 the MIR and can't be used, hence, only light directed within a narrow internal cone with $\theta_c \approx 18^\circ$ given by the high
129 index substrate to air interface can be extracted. The out-coupling efficiency can be improved by either increasing θ_c
130 (e.g. by means of surface structuring or plasmonic metasurfaces [4, 5]) or by redirecting the remainder light into the
131 escape cone. This can be achieved by employing sidewall reflectors, backside structuring or constructive interference
132 at normal incidence [6]. The latter makes use of the fact, that in ICLEDs the photons are generated in precisely
133 located active stages which can be treated as planes of randomly distributed oscillating dipoles. In close vicinity to
134 the metal mirror on the backside (and for light at normal incidence) the upward-radiated electric far field for each
135 dipole arises from interference with the reflected light. At normal incidence the electric field amplitude
136 $E^2 \propto \cos(2kz)$ forms nodes and antinodes as shown in figure 1, with no necessity of a Fabry-Perot cavity.
137 Constructive interference can boost the photon extraction efficiency up to a factor of two compared to uniform stage
138 placement [6].

139
140 Figure 2 presents the L-I-V characteristics of three different ICLED configurations, each with $d = 640 \mu\text{m}$ at ambient
141 temperature, in which constructive (destructive) interference was realized by positioning the active stages in the
142 electric field's antinodes (nodes). The devices were characterized in pulsed mode (500 ns pulses, 10 kHz repetition)
143 on wafer level using a fully automated LED wafer prober. This setup is equipped with a transparent GaAs sample
144 carrier, since light is emitted downwards through the substrate. Each curve represents the average of 40 to 50
145 measured devices.

146 The voltage profile of both stage-separated (3x3) ICLEDs is almost identical, which is plausible since the only
147 difference is a change in thickness of the upmost GaSb spacer layer. However, the voltage drop over the (1x9) device
148 is considerably smaller, since less transition layers between the groups of active stages and GaSb spacer layers with
149 their respective conduction band offset have to be overcome by the carriers.

150 The output power shows the MIR typical sublinear progression, due to non-radiative Auger recombination,
151 increasing more rapidly with injected carrier density than the radiative rate [7]. At operating currents of 380 mA, the
152 output power for constructive interference is around two-times higher than for destructive interference, even though
153 destructive interference only truly vanishes under ideal conditions, namely monochromatic light, normal incidence
154 and without dispersion as shown in figure 3. The cw emission spectra were measured at $T = 20^\circ\text{C}$ with injection
155 currents of 200 mA and each spectrum's intensity was adjusted so that its integral corresponds to the total output
156 power of the device. The node sample reaches a minimum in spectral intensity for the targeted wavelength of 3.5
157 μm . The distortions at 4.3 μm in all three intensity curves result from CO₂ absorption.

158 Especially the spectral FWHM of $\sim 700 \text{ nm}$ is causing the electric field intensity distribution to smear out, which is
159 why stage groups and spacers should not be too narrow. It must also be noted that the target peak wavelength of 3.5
160 μm is slightly off, which affects the correlation between group spacing and peak wavelength. The design with one
161 block of 9 stages is spanning a longer distance, making it less susceptible to electric field intensity broadening and
162 deviations from the targeted wavelength, resulting in the highest output power.

163
164 Apart from reflection losses, one of the main limitations for extracting the generated photons from substrate emitting
165 ICLEDs is the absorption in the highly Te doped GaSb substrate. The free-carrier absorption by electrons is one of
166 the dominating (optical) sub-bandgap absorption mechanisms at room temperature and prevents the generated
167 photons from reaching the substrate-to-air interface. Related to gallium vacancies and gallium antisites and
168 irrespective of growth technique and conditions, nominally undoped GaSb is always p-type in nature resulting in a
169 residual carrier concentrations of about 10^{17} cm^{-3} [8].

171 To improve the optical transparency it is essential to reduce the native acceptors e.g. by lithium diffusion or by
172 tellurium doping compensation which was firstly reported by Milvidskaya et al. [9]. The latter technique makes it
173 crucial to grow a highly doped GaSb layer in order to form ohmic contacts at the substrate side of the active region.
174 To investigate the effects of impurity compensation, two samples with a 3x3 active stage design were grown. One on
175 an n-type GaSb substrate ($n > 5 \cdot 10^{17}/\text{cm}^3$) and one on a low doped substrate that requires the mentioned 500 nm
176 Te-doped interstitial layer for the substrate side contact.
177

178 Figure 4 shows a series of pulsed optical measurements of substrate emitting samples which have been thinned down
179 to various thicknesses. The substrates were chemically-polished to achieve comparable substrate-air reflectivities.
180 Consequently the detected output power translates to the transmittance of the substrate. The absorption coefficients
181 of $\alpha=28.4 \text{ cm}^{-1}$ for the non-transparent and 5.5 cm^{-1} for the semi-transparent substrate result directly from the
182 curvature of the transmission distribution. The higher transmittance indicates that an improvement in ICLED light
183 output of 70 % is to be expected for the targeted substrate thickness of 150 μm .

184 The effective parameters from [10] are used to calculate carrier concentrations contributing to the absorption
185 mechanisms. For the highly doped substrate, the residual n-type carrier concentration results in $1.3 \cdot 10^{18}$. The
186 calculation for the semi-transparent substrate is more complex since the measurement does not give any information,
187 which carrier type contributes to which amount to the absorption. Thus, the effective masses and absorption
188 parameters are bound to have rather large errors associated with it leading to an estimated residual carrier
189 concentration in the 10^{17} range.
190

191 The most promising stage configuration concerning light out-coupling and electrical properties is the one with a
192 block of 9 active stages in an antinode of the optical field as shown in Fig. 2. On this basis, ICLEDs with square
193 shaped mesa structures ($d = 640$) were fabricated and thinned down to 150 μm thickness using semi-transparent
194 GaSb substrates. Single emitters were diced and flip-chip mounted on AlN heat spreaders using AuSn, which were
195 subsequently soldered onto a single layer aluminum PCB. The PCB was attached onto a thermoelectrically cooled
196 measurement station. The devices were analyzed in cw mode concerning their temperature dependent L-I-V
197 characteristics and spectral properties (Figure 5). The total output power was measured using an integrating sphere
198 with a thermoelectric cooled HgCdTe detector. In addition to Auger recombinations, also lattice heating contributes
199 to the L-I rollover at high drive currents. The maximum cw output power was $\sim 5.1 \text{ mW}$ at $T=20^\circ\text{C}$ with a
200 corresponding voltage drop of 5.1 V. Even though no AR coating was used, this result is higher than any previously
201 reported values for MIR LEDs operating at ambient temperature.

202 The maximum output power at $T=20^\circ\text{C}$ corresponds to an intensity of $1.25 \text{ W}/\text{cm}^2$, which is less than the reported
203 maximum for smaller, circular shaped ICLEDs [3] ($2.3 \text{ W}/\text{cm}^2$). This difference can be assigned to the lower number
204 of cascades. Even higher intensities have been reported by Koerperick et al [11], although at cryogenic temperatures
205 where radiative lifetimes are decreased and non-radiative lifetimes increased. Figure 5 displays the WPE at $T=20^\circ\text{C}$
206 as function of driving current, which is one of the most important performance indicator for LEDs. The maximum
207 WPE $\sim 0.7 \%$ can be achieved at a driving current of 24 mA and a corresponding emittance of $0.1 \text{ W}/\text{cm}^2$. The
208 WPE ranges from $\sim 0.7 \%$ at low powers to $\sim 0.2 \%$ at the maximum power. This is 2-3 times higher than the
209 previous reported values which were in the range of 0.05 to 0.4 %. The improvement in WPE is attributed to the
210 lower doping of the substrate. The great advantage especially at high driving currents is a consequence of the rather
211 large active area, leading to a lower current density of $147 \text{ A}/\text{cm}^2$ compared to $478 \text{ A}/\text{cm}^2$ at 600 mA and
212 consequently to less Auger recombinations.

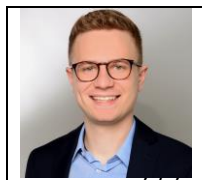
213 We expect further improvements by enhancing the light out-coupling efficiency through surface texturing such as
214 motheye patterns that broaden the internal cone of the emitted light. Metasurface antennas could also be a suitable
215 candidate, since they are not bound to the limitations of total internal reflection, when refracting the emitted light.
216 Moreover the spatial phase variation enables to effectively control the direction and shape of the refracted wavefront.
217

218 In conclusion, ICLEDs were realized that yield higher output powers and WPEs than any previous MIR LEDs
219 operating at ambient temperature. The maximum cw output power when operating at 20°C is 5.1 mW , the WPE
220 ranges from 0.17 to 0.7%. The advantage over previous ICLEDs can be attributed to stage grouping at one single
221 antinode of the optical field and the usage of low absorbing substrates. We expect further improvements by
222 optimizing the GaSb spacer thickness in order to tune the active stages more precisely to the peak wavelength
223 position. The demonstrated concept is, in principle, compatible to ICLED arrays and efficient emission at longer
224 wavelengths extending into the longwave infrared.
225
226
227

228 References

229
230 1. Dong, Lei, et al. "Ppb-level formaldehyde detection using a CW room-temperature interband cascade laser
231 and a miniature dense pattern multipass gas cell." *Optics express* 23.15 (2015): 19821-19830.
232
233 2. Vurgaftman, I., et al. "Interband cascade lasers." *Journal of Physics D: Applied Physics* 48.12 (2015):
234 123001.
235
236 3. Kim, Chul S., et al. "Improved mid-infrared interband cascade light-emitting devices." *Optical Engineering*
237 57.1 (2017): 011002.
238
239 4. Chen, Luzhou, et al. "Simultaneous enhancement of light extraction and spontaneous emission using a
240 partially reflecting metasurface cavity." *Physical Review A* 95.5 (2017): 053808.
241
242 5. Danilova, T. N., et al. "Light-emitting diodes based on GaSb alloys for the 1.6–4.4 μm mid-infrared spectral
243 range." *Semiconductors* 39.11 (2005): 1235-1266.
244
245 6. Benisty, H., Hans De Neve, and Cl Weisbuch. "Impact of planar microcavity effects on light extraction-Part
246 I: Basic concepts and analytical trends." *IEEE Journal of quantum electronics* 34.9 (1998): 1612-1631.
247
248 7. Vurgaftman, I., et al. "Rebalancing of internally generated carriers for mid-infrared interband cascade lasers
249 with very low power consumption." *Nature communications* 2 (2011): 585.
250
251 8. Dutta, P. S., Bhat, H. L., & Kumar, V. (1997). The physics and technology of gallium antimonide: An
252 emerging optoelectronic material. *Journal of applied physics*, 81(9), 5821-5870.
253
254 9. Milvidskaya, A. G., et al. "The properties of heavily compensated high resistivity GaSb crystals." *Materials*
255 *Science and Engineering: B* 22.2-3 (1994): 279-282.
256
257 10. Chandola, A., R. Pino, and P. S. Dutta. "Below bandgap optical absorption in tellurium-doped GaSb."
258 *Semiconductor Science and Technology* 20.8 (2005): 886.
259
260 11. Koerperick, Edwin J., et al. "High-power MWIR cascaded InAs–GaSb superlattice LEDs." *IEEE Journal of*
261 *Quantum Electronics* 45.7 (2009): 849-853.
262
263

264 Biographies



265 **Nicolas Schäfer** received his BS and his MS degree from the Karlsruhe Institute of Technology in
266 2014 and 2016, respectively, both in physics. He joined the R&D division at nanoplus
Nanosystems and Technologies GmbH in 2017, an ISO 9001 and 14001 certified supplier of
semiconductor devices and lasers for trace gas sensing. His research interests are in the area of
MID-IR light emitting diodes.

273



274 **Julian Scheuermann** received his Dipl Ing degree in nanotechnology engineering from the
275 University of Würzburg, Germany, in 2012. He then joined nanoplus Nanosystems and
276 Technologies GmbH and is now working in the R&D division on advanced laser sources for
277 spectroscopic applications. His research interests are in the area of innovative MID-IR interband
278 cascade-based light sources.

280



286

Robert Weih received his Dipl Ing degree in nanotechnology engineering and PhD degree in Physics from the University of Würzburg in 2011 and 2018, respectively. In 2015, he joined the epitaxy division at nanoplus Nanosystems and Technologies GmbH, an ISO 9001 and 14001 certified supplier of semiconductor devices and lasers for trace gas sensing. His research interests are in the area of molecular beam epitaxy for innovative MID-IR laser and detector structures.

287



293

Johannes Koeth received his Dipl Phys and PhD degree from the University of Würzburg in 1996 and 2002, respectively, all in physics. In 1998, he cofounded nanoplus Nanosystems and Technologies GmbH and has been the CEO of the company ever since. His research interests have been in the area of molecular beam epitaxy and innovative semiconductor laser structures. He authored around 150 publications of innovative semiconductor devices and their applications in sensing.

294



301

Sven Hoefling received his Diploma in applied physics from the University of Applied Science Coburg, Germany. In 2003, he joined the Department Technische Physik, University of Würzburg, for his PhD work on single-mode emitting quantum cascade lasers. He is a professor in physics and holds a personal chair at Würzburg University, and the University of St. Andrews, Scotland, since 2015 and 2013, respectively. His research is concerned with the design, fabrication, and characterization of lowdimensional electronic and photonic structures.

302

303

304

List of figure captions

305

306

Fig. 1 Schematic of flip-chip mounted ICLEDs with 9 active stages in three different configurations: centered on an antinode (a), split into 3 groups positioned at nodes (b), split into 3 groups positioned at antinodes (c) of the optical field reflected from the backside metallization.

307

308

309

310

Fig. 2 L-I-V characteristics of ICLEDs with mesa edge length of 640 μm measured in pulsed mode (500 ns pulses, 10 kHz repetition). The 9 active stages were positioned in different configurations to investigate the impact of constructive or destructive interference.

311

312

313

314

Fig. 3 cw emission spectra for flip-chip mounted ICLEDs with mesa edge length of 640 μm at the fixed current of 200 mA. Constructive (destructive) interference at a wavelength of around 3.5 μm was realized by positioning the active stages in the electric field's antinodes (nodes).

315

316

317

318

Fig. 4 transmission distribution resulting from pulsed optical measurements (500 ns pulses, 10 kHz repetition) of two substrate emitting ICLEDs at fixed currents of 200 and 300 mA. The ICLEDs were grown on low / high doped substrates and were thinned down to various thicknesses.

319

320

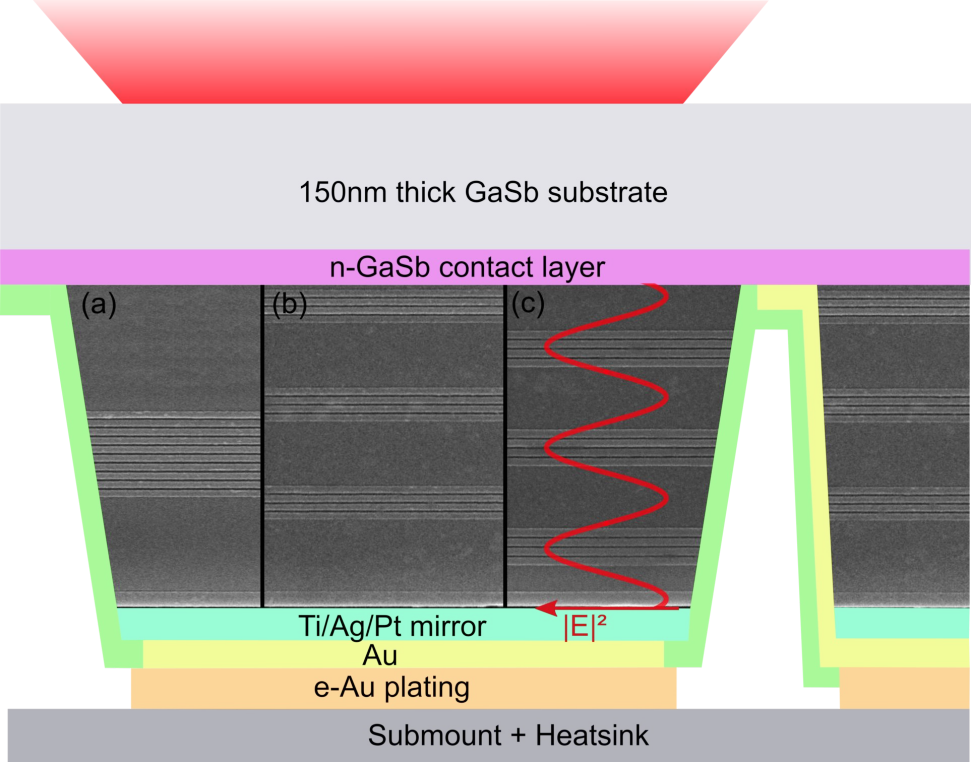
321

322

Fig. 5 cw L-I-V characteristics for a flip-chip mounted ICLED with 1x9 active stages and mesa edge length of 640 μm at seven different temperatures ranging from 0°C to 70°C.

323

324



A cross-sectional diagram of a device structure. At the top, a red trapezoidal shape represents an incident light beam. Below it is a grey layer labeled "150nm thick GaSb substrate". Underneath is a purple layer labeled "n-GaSb contact layer". The main body of the device is a dark grey region with horizontal lines, divided into three sections labeled (a), (b), and (c) by vertical black lines. Section (c) contains a red wavy line representing an electromagnetic wave. Below this region is a light blue layer labeled "Ti/Ag/Pt mirror". Underneath the mirror is a yellow layer labeled "Au", and below that is an orange layer labeled "e-Au plating". The entire structure is supported by a grey base labeled "Submount + Heatsink".

150nm thick GaSb substrate

n-GaSb contact layer

(a)

(b)

(c)

Ti/Ag/Pt mirror

Au

e-Au plating

$|E|^2$

Submount + Heatsink

